SLAC-PUB-1862
LBL-5595
December 1976
(T/E)

MESONIC DECAYS OF THE $\psi(3095)$*

F. Vannucci†, G. S. Abrams, M. S. Alam, A. M. Boyarski, M. Breidenbach, W. Chinowsky, G. J. Feldman, C. E. Friedberg, D. Fryberger, F. J. Gilman, G. Goldhaber, G. Hanson, J. A. Jaros, B. Jean-Marie‡, J. A. Kadyk, R. R. Larsen, D. Lüke††, V. Lüth, H. L. Lynch, R. J. Madaras, C. C. Morehouse‡‡, H. K. Nguyen§, J. M. Paterson, I. Peruzzi†, M. Piccolo†, F. M. Pierre‡, T. P. Pun, P. Rapidis, B. Richter, B. Sadoulet, R. F. Schwitters, W. Tanenbaum, G. H. Trilling, J. S. Whitaker, J. E. Wiss

Lawrence Berkeley Laboratory and Department of Physics
University of California, Berkeley, California 94720

and

Stanford Linear Accelerator Center
Stanford University, Stanford, California 94305

ABSTRACT

We present branching ratios for several mesonic decay modes of the $\psi(3095)$. The two-body and quasi-two-body final states have branching ratios that follow the general pattern of behavior expected for the decay of an SU(3) singlet via an SU(3) symmetric interaction. The $\pi^+\pi^-$ and K^+K^- mass spectra in $\omega\pi\pi$, ωKK, $\phi\pi\pi$, and ϕKK final states show remarkable differences that are most readily interpretable in terms of the Okubo-Zweig-Iizuka Rule.

(Submitted to Phys. Rev.)

*Work supported by the Energy Research and Development Administration.
†Permanent address: Institut de Physique Nucléaire, Orsay, France.
‡Permanent address: Laboratoire de l'Accélérateur Linéaire, Orsay, France.
††Fellow of Deutsche Forschungsgemeinschaft.
Permanent address:
‡‡Varian Associates, Palo Alto, California.
§LPNHE, Université Paris VI, Paris, France.
+Laboratori Nazionali, Frascati, Rome, Italy.
≠Centre d'Études Nucléaires de Saclay, France.

I. INTRODUCTION

The remarkably narrow width of the $\psi(3095)$, hereafter denoted by the symbol ψ, is now usually interpreted by considering the ψ as a bound state of two charmed quarks ($c\bar{c}$) whose decay is inhibited because it violates the Okubo-Zweig-Iizuka (OZI) rule.[1] The recent discovery of states most naturally interpreted as charmed mesons gives considerable support to this interpretation.[2] It is of interest to study in some detail various specific hadronic decay modes of the ψ to determine whether branching ratios and other properties are those expected from a $c\bar{c}$ bound state, and to what extent SU(3) symmetry is satisfied in the decay process. In this connection it is worth noting that the relatively high mass and small angular momentum of the ψ substantially reduce the barrier and phase space corrections usually needed in applying SU(3) to conventional hadron spectroscopy, and the study of ψ decays thus affords new opportunities to check this symmetry.

We have already reported[3] studies of multipion decays of the ψ, which established that (1) isospin is conserved in ψ hadronic decays and (2) the ψ has isospin zero as expected from the $c\bar{c}$ model. As we noted, a significant fraction of the ψ decays occur via the emission and reabsorption of an intermediate photon (second-order electromagnetic process). These presumably reflect the isospin and SU(3) properties of the photon rather than the ψ and their effect needs to be considered in the interpretation of the ψ decays.

In this paper we present measurements of branching ratios for a number of exclusive mesonic decay channels of the ψ, with particular emphasis on channels with kaons. We then interpret these results in terms of the expectations from SU(3) symmetry and from further application of the OZI rule.

II. EXPERIMENTAL DETAILS

The data presented in this paper are based on the analysis of approximately 150,000 hadronic decays of the ψ recorded by the SLAC-LBL magnetic detector operating at the SLAC electron-positron colliding-beam facility, SPEAR. This sample corresponds to an integrated luminosity of 140 nbarn^{-1}.

The general properties of the detector have been described elsewhere,[4] but it may be useful to summarize the relevant elements here. Figure 1 shows a cross section of this instrument. The momenta and directions of charged particles produced in the collision region (including those from the decay of neutral strange particles) are measured in two cylindrical proportional chambers and four sets of cylindrical wire spark chambers, all immersed in a solenoidal magnetic field of about 4 kG extending over a region 3m in diameter and 3m in length. The whole system is concentric with respect to the e^+e^- beam axis. Each set of wire spark chambers has two gaps (4 wire planes). The wires are inclined $\pm 4^\circ$ with respect to the beam axis in one gap and $\pm 2^\circ$ in the other gap, thus providing both two-dimensional spatial information and ambiguity resolution. A set of 48 2.5-cm thick plastic scintillation counters at a radial distance of 1.5m from the axis, just inside the solenoid coil, provides trigger signals and time-of-flight information (TOF) for particle identification. The rms resolution of this TOF system is 0.4 ns. Outside the coil a cylindrical array of 24 lead-scintillator shower counters is used for electron identification (large pulse height) as well as for the detection of particles necessary for the trigger. The detector accepts the full azimuth and a range of polar angles extending from 50° to 130°. A 20-cm thick iron magnetic flux return lies outside the shower counters and serves also as a hadron filter for muon identification. One or more planar wire spark chambers are outside the flux return over about 70% of the

azimuth. Additional muon detection is provided by a tower above the main detector, consisting of two 66-cm thick slabs of baryite-loaded concrete, each followed by wire spark chambers. The muon tower covers about 15% of the azimuth.

The trigger requirement demands two or more charged particles as manifested by signals in two TOF counters and associated shower counters and signals from a cylindrical counter close to the beam pipe in coincidence within the beam crossing time. The beams consist of a single electron bunch and a single positron bunch colliding over a time interval of about 0.2 ns; the period between successive collisions in a particular interaction region is 780 ns. For tracks coming from the beam interaction region (which is then used as part of the trajectory) the typical momentum precision is about 1.5% at 1 GeV/c. The precision is somewhat lower for tracks that are the decay products of strange particles such as K^o_S.

In order to translate observed rates for particular processes into branching ratios, it is necessary to make substantial corrections to account for finite detector acceptance, trigger efficiency, cuts used for sample selection to diminish background, efficiency of TOF identification, etc. This has been done with a Monte Carlo program in which measurement errors, trigger requirements, and detector geometry have all been introduced to simulate the detector and to take account of the cuts applied to the data. Although the fact that we are considering specific channels removes much of the model dependence of such efficiency calculations, there are decay modes for which such uncertainties remain. These uncertainties have been included in the errors assigned to the corresponding branching ratios. The efficiency of TOF separation of π and K is sensitive to the particle momentum, falling off at momenta above 600 MeV/c.

This introduces additional efficiency corrections for those classes of events in which TOF information is used. For this reason, the TOF information has been used only where it was an essential complement to the kinematical information.

III. BRANCHING RATIO DETERMINATIONS

The results of the branching ratio determinations described in this paper are given in Table I, together with the relevant numbers of events and efficiencies. These efficiencies include both the effects of detector and trigger biases and the branching ratios of the decay modes into the topologies studied. In the following discussion we describe the criteria by which the samples used in these determinations are chosen. The discussion of the results in Table I is given in the next section. We will use the following notation conventions: $K^* \equiv K^*(892)$, $K^{**} \equiv K^*(1420)$, $KK^* \equiv K\bar{K}^* + \bar{K}K^*$, $KK^{**} \equiv K\bar{K}^{**} + \bar{K}K^{**}$, etc.

A. $\psi \to K_S K_L \to (\pi^+\pi^-)$ + Missing Mass

For our sample of two-prong events containing particles of opposite charge, we have computed the invariant mass, assuming both particles to be pions. This mass spectrum, shown in Fig. 2a, shows a clear signal at the K^0 mass. For those events for which $M(\pi^+\pi^-)$ is within ±30 MeV of the K^0 mass, we show in Fig. 2b the spectrum of missing mass recoiling against the candidate K_S. Four events are consistent with the K^0 mass within the experimental resolution. They are compatible with the expected multipion states produced in association with the background underneath the K_S peak in Fig. 2a. The efficiency for detection of the $K_S K_L$ has been obtained by a Monte Carlo calculation in which the $K\bar{K}$ angular distribution was taken to be $\sin^2\theta$ (θ is the polar angle relative to the beam line) as expected for ψ decay into two pseudoscalars. The data of Fig. 2b coupled with this efficiency lead to the rather stringent upper limit of

8.9×10^{-5} for the branching ratio for $\psi \to K_S K_L$.

B. $\psi \to K^+K^-, \pi^+\pi^-$

To identify hadron pairs, it is necessary to remove the large background of lepton pairs. To do this we require: (a) each track point toward at least one muon spark chamber, but that no chamber have a spark in the vicinity of the projected track's trajectory; (b) each track point toward the central 90% of a shower counter, and that the shower have a low pulse height, less than about a third of that expected for an electron.

In addition to requiring that each track be identified as a hadron, we require that they have approximately equal momenta, and that the two tracks be collinear within 50 mrad. We then do a fit to the track trajectories under the constraint that the momenta be equal and opposite. If we further assume that the two hadrons have the same mass, energy-momentum conservation uniquely determines the hadron mass. The square of hadron masses obtained in this way is shown in Fig. 3.

Out of a sample of about 105,000 hadronic events (the muon detection system was not operational for some of the early data) there are three candidates for $\psi \to \pi^+\pi^-$, two candidates for $\psi \to K^+K^-$, and 41 candidates for $\psi \to p\bar{p}$. Each of the five meson pair candidates is within one standard deviation of the favored hypothesis and greater than 1.9 standard deviations from the unfavored hypothesis.

The number of events expected from misidentifications of lepton pairs is 1.26 events for $\pi^+\pi^-$ and 0.23 events for K^+K^-. The evidence that $\psi \to \pi^+\pi^-$ exists is stronger than indicated by the above numbers since one of the $\pi^+\pi^-$ candidates was particularly well identified. In this event, the two shower counter pulse heights were less than one-fifteenth and one-eighth of the expected

pulse heights for electrons, and five separate muon spark chambers, which would be expected to fire if the event were a muon pair, failed to produce an appropriate signal. The presence of fiducials on all muon spark chambers and the detection of muons in preceding and following events indicate that the muon detection system was operating properly. The chance of observing such an event from misidentification of a lepton pair is less than 3%.

The branching ratios for the decay to meson pairs can be most easily calculated by normalizing to the known branching ratio for $\psi \to p\bar{p}$ [5,6,7] and by correcting for

a. the different assumed angular distributions ($\sin^2\theta$ for $\pi\pi$, KK and $1+\cos^2\theta$ for $p\bar{p}$),

b. the probability for a $\bar{p}$ to annihilate and give a large pulse height in a shower counter, and

c. the probability for a charged K to decay in flight.

The branching ratios calculated in this way are $(1.6 \pm 1.6) \times 10^{-4}$ for $\psi \to \pi^+\pi^-$ and $(2.0 \pm 1.6) \times 10^{-4}$ for $\psi \to K^+K^-$. These values agree well with those obtained by the DASP collaboration:[7] $(1.0 \pm 0.7) \times 10^{-4}$ for $\psi \to \pi^+\pi^-$ based on the observation of two events with 0.24 events background and $(1.4 \pm 1.4) \times 10^{-4}$ for $\psi \to K^+K^-$ based on the observation of one event with 0.20 events background.

Since the decay $\psi \to \pi^+\pi^-$ violates isospin conservation,[3] it must occur via a second-order electromagnetic interaction. The decay $\psi \to K^+K^-$ is SU(3) forbidden, as we will discuss in Section V. In addition, to the extent that the $\psi \to K^+K^-$ branching ratio is larger than that for $\psi \to K^0\bar{K}^0$, the excess must be due to a second-order electromagnetic interaction. Assuming that both $\psi \to \pi^+\pi^-$ and $\psi \to K^+K^-$ proceed entirely by this process, their rates relative to

$\psi \to \mu^+\mu^-$ directly measure the electromagnetic form factors of the mesons, $|F_\pi|^2$ and $|F_K|^2$. In the approximation where the muon mass is ignored, these form factors are given by:

$$|F_h|^2 = \frac{4}{\beta_h^3} \frac{\sigma(e^+e^- \to h^+h^-)}{\sigma(e^+e^- \to \mu^+\mu^-)}$$

where h stands for either π or K and σ is the observed production cross section, whether resonant or not. We obtain $|F_\pi|^2 = (8 \pm 8) \times 10^{-3}$ and $|F_K|^2 = (1.2 \pm 1.0) \times 10^{-2}$. A simple ρ pole, $F_\pi = (1 - s/m_\rho^2)^{-1}$, predicts $|F_\pi|^2 = 4.3 \times 10^{-3}$, while a simple ϕ pole predicts $|F_K|^2 = 1.5 \times 10^{-2}$, each consistent with our results.

C. $\psi \to K_S K^\pm \pi^\mp \to (\pi^+\pi^-)K^\pm\pi^\mp$

The population from which the sample is selected consists of charge zero, four-prong events such that the total missing momentum is less than 100 MeV/c. K_S decays are selected by requiring, as before, that $M(\pi^+\pi^-)$ be within ± 30 MeV/c^2 of the K^o mass. To insure that the kinematics are consistent with the $K_S K\pi$ decay mode, and to select which charged track is the kaon, we take that choice of particle identities which minimizes $|M(K_S K\pi) - M_\psi|$ and accept only those events for which that quantity is less than 50 MeV/c^2. The Dalitz plot for this sample of events is shown in Fig. 4. The population is dominated by the two bands corresponding to K^oK^{*o} and $K^\pm K^{*\mp}$. The small grouping of events near the diagonal edge of the Dalitz plot most probably arises from interchanges of the proper charged pion and kaon identifications - when kaon and pion identities are interchanged these same events fall on the $K^{*\pm}$ band. We have assumed in determining branching ratios that they belong to this band, but their contribution is within the quoted uncertainty. It is interesting to note that just as the

$\pi^+\pi^-\pi^0$ channel is dominated by $\rho\pi$,[3] the $K_S K\pi$ channel is dominated by the quasi-two-body final state KK^*. Furthermore it is clear from Fig. 4 that the K^0K^{0*} band has population about equal to that of the $K^{\pm}K^{*\mp}$ band. After correction for relative acceptance the ratio $K^0K^{0*}/K^{\pm}K^{*\mp}$ is 0.84 ± 0.25, in agreement with the value of unity expected from a pure isospin state. Finally it should be noted from Fig. 4 that there is no evidence for the decay modes KK^{**}.

D. $\underline{\psi \to \pi^+\pi^-K^+K^-}$

The population from which we choose our sample consists of charge-zero four-prong events such that the total missing momentum is less than 50 MeV/c. This more stringent limit on missing momentum than the 100-MeV/c cut made in the $K_S K^{\pm}\pi^{\mp}$ channel is justified by the improved momentum resolution arising from the fact that all four tracks can be constrained to come from the beam-beam interaction point; this is of course not permissible for $\pi^+\pi^-$ produced in K_S decay. The resulting group of events consists principally of the channels $\pi^+\pi^-\pi^+\pi^-$, $\pi^+\pi^-K^+K^-$, and $\pi^+\pi^-p\bar{p}$ in roughly comparable proportions. To do further purification, we use the TOF information and compute a χ^2_{TOF} defined as follows:

$$\chi^2_{TOF} = \sum_{tracks} \frac{(t_{pred} - t_{meas})^2}{\sigma^2}$$

where t_{meas} is the measured time of flight for each track, t_{pred} is the predicted time of flight based on a particular set of particle identities, and σ is the TOF measurement uncertainty (0.4 ns). We choose that combination of $\pi^+\pi^-K^+K^-$ which minimizes $\chi^2_{TOF}(\pi\pi KK)$ and consider further only those events for which $\chi^2_{TOF}(\pi\pi KK) < \chi^2_{TOF}(4\pi)$. Figure 5a shows the effective mass $M(\pi^+\pi^-K^+K^-)$ for these events. The χ^2_{TOF} inequality test removes almost all the $\pi^+\pi^-\pi^+\pi^-$ events leaving $\pi^+\pi^-K^+K^-$ (sharp peak at 3100 MeV/c^2 in Fig. 5a)

and $\pi^+\pi^-p\bar{p}$ (broader structure near 2450 MeV/c^2). Imposing a further cut, $|M(\pi\pi KK) - M_\psi| < 50$ MeV/c^2, we finally obtain a very clean $\pi^+\pi^-K^+K^-$ event sample. From that sample, we extract several quasi-two-body and quasi-three-body decay modes.

1. $\psi \to \phi\pi^+\pi^-$. Figure 6a shows the $M(K^+K^-)$ spectrum for the $\pi^+\pi^-K^+K^-$ sample and provides clear evidence for the occurrence of the final state $\phi\pi^+\pi^-$. The $M(\pi^+\pi^-)$ spectrum from this channel, shown in Fig. 7a, is remarkable for the almost total absence of events with $M(\pi^+\pi^-)$ above 1 GeV/c^2, such as ϕf events, a feature which will be further discussed in Section V.

2. $\psi \to K^*\bar{K}^*, K^*K^{**}, K^{**}\bar{K}^{**}$. Figure 8 shows the scatter plot of $M(K^+\pi^-)$ versus $M(K^-\pi^+)$ after removal of the $\phi\pi^+\pi^-$ events. The corresponding $K^\pm\pi^\mp$ projection is shown in Fig. 9. The most prominent features of Fig. 8 are bands corresponding to K^* and $\bar{K}^*$, with accumulations of events indicating substantial production in association with $\bar{K}^{**}$ and K^{**}, respectively. There does not appear to be significant $K^*\bar{K}^*$ or $K^{**}\bar{K}^{**}$ production, although the statistics are too limited to make any strong statement.

E. $\psi \to K^+K^-K^+K^-$

The sample was selected from four-prong, zero-charge events with the usual requirement that the missing momentum be less than 50 MeV/c and the further requirements that at least one of the four particles be clearly identified as a kaon by TOF and that $|M(4K) - M_\psi| < 50$ MeV/c^2. Figure 5b exhibits the spectrum of M(4K) after the above cuts on missing momentum and TOF are made; there is indeed a signal of 19 events near the ψ mass. The shading in Fig. 5b indicates those events in which at least three of the four charged particles are identified as kaons, and strongly supports the $K^+K^-K^+K^-$ identification. The shaded events near 3500 MeV/c^2 are $\pi^+\pi^-K^+K^-$ in which, due to TOF

uncertainties, one of the pions is erroneously identified as a kaon. Figure 6b shows the $M(K^+K^-)$ spectrum (four combinations per event) for the $K^+K^-K^+K^-$ events. A ϕ signal consisting of 14 events is evident. The mass spectrum for the K^+K^- pairs produced in association with the ϕ is shown in Fig. 7c and indicates that for half of the events $M(K^+K^-)$ is between 1500 and 1600 MeV/c^2. This behavior is most naturally interpreted in terms of the quasi-two-body decay mode $\phi f'$.

F. $\psi \to K^+K^-\pi^+\pi^-\pi^o$, $K^+K^-\pi^+\pi^-\eta$

We have accepted into our sample only those four-prong, charge-zero events which satisfy the same χ^2_{TOF} condition as the $\pi^+\pi^-K^+K^-$ events. Furthermore, to remove events without missing neutrals, we further restrict our sample by accepting only events in which the missing momentum exceeds 200 MeV/c. The spectrum of missing mass squared (MM^2), shown in Fig. 10a, has a clear peak corresponding to missing π^o, but no appreciable η signal above the background. We select our $K^+K^-\pi^+\pi^-\pi^o$ events and $K^+K^-\pi^+\pi^-\eta$ candidates by the cuts $-0.05 < MM^2 < 0.09$ $(GeV/c^2)^2$ and $0.25 < MM^2 < 0.35$ $(GeV/c^2)^2$ respectively.

Figures 11a and 11b show, for both of these final states, scatter plots of $M(K^+K^-)$ versus $M(\pi^+\pi^-\pi^o/\eta)$. There appear to be six clear $\phi\eta \to K^+K^-\pi^+\pi^-\pi^o$ and two $\phi\eta' \to K^+K^-\pi^+\pi^-\eta$ events. The former are used to provide a rough measure of the $\phi\eta$ branching ratio, and the latter provide an upper limit to the $\phi\eta'$ branching ratio of the ψ.

Figure 12a shows the $\pi^+\pi^-\pi^o$ mass spectrum for the $K^+K^-\pi^+\pi^-\pi^o$ final state. A small ω signal, corresponding to the ωK^+K^- channel, is observed. The corresponding K^+K^- mass spectrum, shown in Fig. 7d, has no indication of f' production, in contrast with the K^+K^- spectrum from ϕK^+K^- where the f' is the dominant feature (see Fig. 7c).

G. $\psi \to K^+K^-\pi^+\pi^-\pi^+\pi^-$

By cuts entirely similar to those used to obtain the $K^+K^-\pi^+\pi^-$ sample, we have also isolated a sample of $K^+K^-\pi^+\pi^-\pi^+\pi^-$ events. The $M(K^+K^-\pi^+\pi^-\pi^+\pi^-)$ mass spectrum for events satisfying the TOF and missing momentum cuts is shown in Fig. 5c, and exhibits a clear peak at 3100 MeV. The $M(K^+K^-)$ spectrum shown in Fig. 6c exhibits no structure and, in particular, no ϕ signal.

H. $\psi \to \pi^+\pi^-\pi^+\pi^-\pi^0$, $\pi^+\pi^-\pi^+\pi^-\pi^+\pi^-\pi^0$

The branching ratios for the $\pi^+\pi^-\pi^+\pi^-\pi^0$ and $\pi^+\pi^-\pi^+\pi^-\pi^+\pi^-\pi^0$ final states of the ψ have been reported by us previously.[3] Our present sample of such events is constructed by taking four-prong and six-prong charge-zero events and imposing the further requirements that the missing momentum be greater than 200 MeV/c, and the missing mass squared lie between -0.05 $(GeV/c^2)^2$ and 0.09 $(GeV/c^2)^2$. The missing-mass-squared spectrum for four-prong events is shown in Fig. 10b. The $M(\pi^+\pi^-\pi^0)$ spectrum for the $\pi^+\pi^-\pi^+\pi^-\pi^0$ sample (four entries for each event) is shown in Fig. 12b, and exhibits a large ω peak. The spectrum of $M(\pi^+\pi^-)$ recoiling against the ω is shown in Fig. 7b. The f is a prominent partner of the ω. This spectrum can only represent $\pi\pi$ states of even C, even J, and isospin zero; hence no ρ is seen or expected. However, as will be discussed in more detail in Section V, the spectrum is remarkably different from that observed in association with the ϕ (Fig. 7a), exhibiting a dip instead of a peak near 1000 MeV/c^2, and having a large population at $M(\pi^+\pi^-) >$ 1100 MeV/c^2, just where the population associated with the ϕ drops to near zero. Figure 7b also exhibits a broad peak at $M(\pi^+\pi^-) = 500$ MeV. The source of this is unclear, but it may be a broad enhancement in the $\pi\pi$ isoscalar s-wave.

Figures 13a and 13b show the $\pi^+\pi^-$ and $\pi^\pm\pi^0$ mass spectra for the $\pi^+\pi^-\pi^\pm\pi^-\pi^0$ final state. In addition to a K^0 peak (presumably from $K_S^0 K^\pm \pi^\mp \pi^0$ events) in the $\pi^+\pi^-$ system, both mass spectra exhibit strong ρ signals. Figure 13c shows the $\pi^\pm\pi^0$ spectrum for those events in which $M(\pi^+\pi^-)$ for any combination of the remaining pions is in the ρ band ($700 < M(\pi^+\pi^-) < 800$ MeV/c^2). This selection enhances the $\rho^\pm$ signal. Finally Fig. 14 shows the $\rho\pi$ mass spectrum for all events of the type $\rho^0\rho^\pm\pi^\mp$, where the above defined mass band is used to select ρ^0 and $\rho^\pm$. A significant peak at 1300 MeV, with the appropriate width of about 100 MeV, is most naturally interpreted as the production of A_2 in the decays

$$\psi \to \rho^0 A_2^0 \to \rho^0 \rho^\pm \pi^\mp$$

$$\to \rho^\pm A_2^\mp \to \rho^\pm \rho^0 \pi^\mp \ .$$

The missing-mass-squared spectrum for six-prong, charge-zero events with missing momentum greater than 200 MeV/c is shown in Fig. 10c. The same missing mass cuts as above define a substantial sample of $3\pi^+3\pi^-\pi^0$ final states. The corresponding $M(\pi^+\pi^-\pi^0)$ spectrum (nine entries per event) is shown in Fig. 12c, and also exhibits a significant ω peak.

IV. GENERAL DISCUSSION OF BRANCHING RATIOS

It is clear from Table I that the ψ decays into a vast number of different mesonic decay modes with fairly small branching ratios for any particular mode. Of all the explicit final states listed in the table, the $2(\pi^+\pi^-)\pi^0$ has the largest branching ratio, namely $(4.0 \pm 1.0)\%$.

It is of some interest to examine what can be inferred from the specific observed states about the population of states with the same particle

multiplicities, but different (and unobservable) charge combinations. Thus, for example, the $2(\pi^+\pi^-)\pi^0$ branching ratio can be used to estimate the branching ratio for the totality of (5π) final states. For this purpose we use the known zero isospin of the $\psi(3095)$ and isospin conservation in the decay process to calculate rigorous limits for the ratio of events of the observed multiplicity and charge state to events of the same multiplicity and all charge states.[8,9] These limits, for the topologies listed in Table I, are given in the third column of Table II. The fourth column of Table II gives corresponding estimates of branching ratios for states of fixed multiplicity independently of the relative numbers of charged and neutral particles. For many of the decays, the range of allowed values is rather broad. We can obtain a unique prediction by using the statistical model in which all available isospin states are populated with their statistical weights.[10] Columns 5 and 6 in Table II list the predictions of the statistical model. This model is an estimate of the most likely value of the ratio of the observed charge state to the corresponding general mode. We have not included in Table II those final states corresponding to an even number of pions, since they presumably arise from a second-order electromagnetic decay of the ψ and do not correspond to isospin zero. We do assume that, for the decays listed in Table II, the electromagnetic contribution to the decay can be neglected.

The sum of all the lower limits given in Table II amounts to $21.6 \pm 2.4\%$, which then represents a lower limit to the ψ branching ratio contribution from the decay topologies discussed in this paper. The statistical model predicts a contribution from these topologies of $30.2 \pm 3.3\%$. This number is to be compared to 69%, the total branching ratio for decay modes which do not arise from

the second-order electromagnetic process.[11] The difference between the 69% and 30% presumably arises from: (i) the contributions from higher multiplicities; (ii) the baryonic decay modes; (iii) decay modes involving η's and/or photons.

V. TESTS OF SU(3) SYMMETRY AND THE OZI RULE

A. SU(3) Classification of the ψ

With the isotopic spin of the ψ established as being zero,[3] i.e., an SU(2) singlet, it is natural to consider its classification under the larger symmetry of SU(3). Relevant information can be obtained from a study of ψ branching ratios into various channels related by SU(3), provided that the decay process itself conserves SU(3). Since the total decay width of the ψ is enormously suppressed compared to typical hadronic widths, we do not necessarily expect the same situation with regard to SU(3) symmetry violation found in other hadronic decays.[12]

In general, the ψ could be an SU(3) singlet, the eighth component of an octet, a member of some higher dimensional representation, or a mixture of the above. If it can be considered as a bound state of a charmed quark and an antiquark, it must be an SU(3) singlet. However, an SU(3) singlet with odd charge conjugation (like the ψ) is forbidden to decay into two mesons belonging to the same SU(3) multiplet, and more generally to decay into members of two multiplets whose $I_3 = Y = 0$ members have the same charge conjugation quantum number.[13] SU(3) symmetry thus forbids the decay of such a singlet into $K\bar{K}$, $K^*\bar{K}^*$, $K^{**}\bar{K}^{**}$, and KK^{**} ($KK^{**} \equiv K\bar{K}^{**} + \bar{K}K^{**}$), while it allows modes such as KK^* and K^*K^{**}. This is generally not true for other SU(3) assignments for the ψ.

Our results, as shown in Table I, are completely compatible with this pattern of forbidden and allowed modes. In particular, the suppression of the

$K_S K_L$ branching ratio, by at least an order of magnitude below those observed for KK* or K*K**, strongly indicates that SU(3) is operative and that the ψ behaves like a singlet.

Further tests of a possible SU(3) singlet assignment involve the comparison of the branching ratios for observed decays into different members of the same two SU(3) multiplets.[13,14] For example, a pure SU(3) singlet couples equally to $\pi^-\rho^+$, $\pi^o\rho^o$, $\pi^+\rho^-$, K^+K^{*-}, $K^o\bar{K}^{*o}$, K^-K^{*+}, $\bar{K}^oK^{*o}$, and $\eta^8\omega^8$, where η^8 and ω^8 denote the pure octet components. Zero isospin for the ψ already requires equality of the rates for the three charge states of the $\pi\rho$ mode and for the four KK* decay channels, which is consistent with our data in Ref. 3 and Table I, respectively.

After correction for p-wave phase space and ϕ-ω (ideal) mixing (the η is taken as a pure octet state), the singlet assignment translates into predicted relative rates for ψ decay into $\pi^+\rho^-$, $K^+\bar{K}^{*-}$, and $\eta\phi$ of 1 : 0.85 : 0.50. The relative experimental branching ratios computed from Table I are

$$2.1 \pm 0.5 : 0.8 \pm 0.15 : 0.5 \pm 0.3 .$$

Results from DASP on the $\pi^\pm\rho^\mp$ and $K^\pm K^{*\mp}$ branching ratios,[7] and from DESY-Heidelberg on the $\pi^\pm\rho^\mp$ branching ratio,[15] obtained by very different techniques, agree within errors with our experimental results.

In general, before comparing the relative experimental rates with the predictions for the direct decays of an SU(3) singlet, one must take into account the possibility of interference with the second order electromagnetic decay of the ψ proceeding through a virtual photon. But in the case of $\pi^+\rho^-$ and $K^+\bar{K}^{*-}$, assuming SU(3) conservation for the virtual photon couplings, the same relative amplitudes are predicted for decays through one photon and direct decays of a singlet state. The ratio of $\pi^+\rho^-$ to K^+K^{*-} is thus unchanged by such an

interference. Furthermore, the observed equality of the rates for $K^{\pm}K^{*\mp}$ and $K^{o}K^{*o}$ (see Table I) argues against a substantial contribution from the second-order electromagnetic process.

The disagreement of the relative branching ratios for $\pi^{+}\rho^{-}$ and $K^{*+}K^{*-}$ with the prediction for a singlet ψ is at the two standard deviation level. If we assume that SU(3) is broken in the decay process with a resulting admixture of a small octet amplitude, A_8, into the dominant singlet amplitude, A_1, for the pseudoscalar-vector final state, the relative rates (corrected for phase space) for $K^{+}K^{*-}$ and $\pi^{+}\rho^{-}$ are proportional to $|A_1-A_8|^2$ and $|A_1+2A_8|^2$, respectively. Our measured branching ratio then yields

$$\mathrm{Re}(A_8/A_1) = 0.15 \begin{matrix} +\,0.07 \\ -\,0.08 \end{matrix}$$

Such a magnitude of symmetry breaking at the 10 to 20% level in the amplitude is consistent with that found in the decays of other mesons and baryons,[10] and agrees with the DASP result[7] of $\mathrm{Re}(A_8/A_1) = +\,0.07 \pm 0.06$.

Another test of an SU(3) singlet assignment for the ψ is possible using the decays into a vector plus tensor meson in Table I. Aside from phase space corrections, decays into each charge state of ρA_2 and K*K** are predicted to occur at equal rates. To relate these uniquely to the ωf or $\phi f'$ decays, we need an additional assumption, since the ideal mixing of the ω-ϕ and f-f' allows another amplitude, that for decay into two SU(3) singlets, to be involved. A negligible ψ decay rate into $\omega f'$ or ϕf, as indicated experimentally (see Section III) and theoretically (by the OZI rule), forces the amplitude for decay into two singlets to be equal to that for decay into two octets and consequently equal amplitudes for $\rho^{o}A_2^{o}$, $K^{*o}\bar{K}^{**o}$, ωf, and $\phi f'$.

With an appropriate correction for s-wave phase space, we then have the prediction for the relative rates for ψ decay into $\rho^{o}A_2^{o}$, $K^{*o}\bar{K}^{**o}$, ωf, and $\phi f'$ of

$$1 : 0.90 : 1.01 : 0.78 .$$

Table I, assuming equal rates into each charge substate of ρA_2 and K^*K^{**}, gives relative ratios of

$$1.0 \pm 0.5 : 1.8 \pm 0.5 : 0.7 \pm 0.3 : 0.3 \pm 0.2 .$$

Given the estimated errors and the possibility of some interference with the amplitude for ψ decay through a virtual photon into these channels, these decay rates, and particularly those for ρA_2 and K^*K^{**}, are consistent with those expected for a singlet state.

In summary, the observation of ψ decays into two mesons belonging to SU(3) multiplets whose $I_3 = 0$ members have opposite values of C, while decays into two mesons in SU(3) multiplets whose $I_3 = 0$ members have the same value of C are not seen, leads one to an SU(3) singlet assignment for the ψ. The relative rates for decays into pseudoscalar plus vector or vector plus tensor mesons generally are in accord with this, although a small amount of symmetry breaking in the decay process seems to be required particularly in pseudoscalar-vector decays. We conclude that the weight of evidence, particularly the pattern of observed and unobserved decays, favors the ψ being an SU(3) singlet.

B. The Okubo-Zweig-Iizuka Rule in ψ Decays

One striking feature of the data is the presence of the decays $\psi \to \omega f$ and $\psi \to \phi f'$, while the similar decays $\psi \to \omega f'$ and $\psi \to \phi f$ are not observed. From Table I we have:

$$\frac{\Gamma(\psi \to \omega f)}{\Gamma(\psi \to \text{all})} = (1.9 \pm 0.8) \times 10^{-3}$$

$$\frac{\Gamma(\psi \to \omega f')}{\Gamma(\psi \to \text{all})} < 1.6 \times 10^{-4} \text{ (90\% c.l.)}$$

$$\frac{\Gamma(\psi \to \phi f)}{\Gamma(\psi \to \text{all})} < 3.7 \times 10^{-4} \text{ (90\% c.l.)}$$

$$\frac{\Gamma(\psi \to \phi f')}{\Gamma(\psi \to \text{all})} = (0.8 \pm 0.5) \times 10^{-3}$$

In the standard quark model with ideal mixing, the ω and f are made up of non-strange quarks, while the ϕ and f' are made up of strange quarks. Thus the observed decays $\psi \to \omega f$ and $\psi \to \phi f'$ correspond to a quark diagram with only one disconnection, while the unobserved decays $\psi \to \omega f'$ and $\psi \to \phi f$ only correspond to doubly disconnected diagrams. This suggests that while all these decays are suppressed by the OZI rule, just as are all strong decays of the ψ, the decays corresponding to <u>doubly</u> disconnected diagrams, such as $\psi \to \phi f$ and $\psi \to \omega f'$, are suppressed by an additional factor.

More information is found by comparing the overall rate for $\psi \to \phi\pi^+\pi^-$, which must correspond to a doubly disconnected diagram, and that for the similar decay $\psi \to \omega\pi^+\pi^-$, which can correspond to singly disconnected diagrams. From Table I we extract the ratio,

$$\frac{\Gamma(\psi \to \phi\pi^+\pi^-)}{\Gamma(\psi \to \omega\pi^+\pi^-)} = 0.21 \pm 0.10 \ .$$

While the decay rate for $\psi \to \phi\pi^+\pi^-$ does appear to be somewhat suppressed compared to that for $\psi \to \omega\pi^+\pi^-$, the degree of suppression is much less than that found, for example, in the case of the $\phi\rho\pi$ coupling constant squared (corresponding to a singly disconnected diagram) compared to the $\omega\rho\pi$ coupling constant squared (corresponding to a connected quark diagram). The upper limit on the branching ratio for $\psi \to \phi\pi^+\pi^-\pi^+\pi^-$, compared to the observed rate for $\psi \to \omega\pi^+\pi^-\pi^+\pi^-$ in Table I, is consistent with there being at least as much suppression of $\phi\pi\pi\pi\pi$ relative to $\omega\pi\pi\pi\pi$ as there is of $\phi\pi\pi$ relative to $\omega\pi\pi$.

However, care must be taken in comparing the overall rates for $\psi \to \phi\pi^+\pi^-$ and $\psi \to \omega\pi^+\pi^-$ as a measure of the suppression due to a doubly rather than singly disconnected quark diagram. We see by comparing Figs. 7a and 7b that the $\pi\pi$ mass distributions are very different in the two decays. In particular, almost the entire $\psi \to \phi\pi^+\pi^-$ channel has dipion masses below $K\bar{K}$ threshold, with a maximum just below 1 GeV.

The dynamics of the $\pi\pi$ system associated with a ϕ is then manifestly different from that associated with an ω. One possible mechanism to understand the spectra and relative rate is the assumption that in ψ decays a ϕ meson is produced dominantly in association with a resonant state containing a strange quark-strange antiquark component. Such a decay process corresponds to singly disconnected quark diagrams, just as does $\psi \to \omega\pi\pi$, so that there should be no relative suppression because of the OZI rule. When the mass of the resonance (e.g., the ϵ or S) is less than two kaon masses, it is forced to decay into $\pi\pi$, even if the strange quark-antiquark component is dominant. When the mass of the resonance is greater than $2M_K$, decay into $K\bar{K}$ becomes possible and dominant for a resonance consisting of mostly a strange quark and antiquark (e.g., the f'). The relative suppression of $\phi\pi\pi$ is thus only moderate for dipion masses below $2M_K$. But for dipion masses above ~ 1 GeV, the magnitude of the $\omega\pi\pi$ compared to $\phi\pi\pi$ signal and the experimental presence or absence of f and f' produced with an ω or ϕ supports in this regime a substantial suppression of ψ decays which correspond to quark diagrams which are doubly rather than singly disconnected.

REFERENCES

1. S. Okubo, Phys. Lett. 5, 165 (1963); G. Zweig, CERN preprints TH401 and TH412 (1964), unpublished; J. Iizuka, Suppl. Prog. Theor. Phys.

37-38, 21 (1966).

2. G. Goldhaber et al., Phys. Rev. Lett. 37, 255 (1976); I. Peruzzi et al., Phys. Rev. Lett. 37, 569 (1976).

3. B. Jean-Marie et al., Phys. Rev. Lett. 36, 291 (1976).

4. J.-E. Augustin et al., Phys. Rev. Lett. 34, 233 (1975).

5. G. Goldhaber, LBL Report LBL-4884 (1976).

6. L. Criegee et al., DESY Report 75/32 (1975).

7. W. Braunschweig et al., Phys. Lett. 63B, 487 (1976).

8. I. M. Shmushkevich, Dokl. Akad. Nauk SSSR 103, 235 (1955).

9. A. Pais, Phys. Rev. Lett. 32, 1081 (1974). Also see M. Peshkin and J. L. Rosner, Institute for Advanced Study preprint COO 2220-93 (1976).

10. A. Pais, Ann. Phys. (N.Y.) 9, 548 (1960).

11. A. M. Boyarski et al., Phys. Rev. Lett. 34, 1357 (1975).

12. N. P. Samios, M. Goldberg, and B. T. Meadows, Rev. Mod. Phys. 46, 49 (1974).

13. H. Harari, Stanford Linear Accelerator Report No. SLAC-PUB-1514 (1974). F. J. Gilman, in AIP Conference Proceedings, No. 26, High Energy Physics and Nuclear Structure - 1975, Los Alamos, 9-13 June 1975, ed. D. E. Nagle, R. L. Burman, B. G. Storms, A. S. Goldhaber, and C. K. Hargrave (American Institute of Physics, New York, 1975), p. 331. V. Gupta and R. Kogerler, Phys. Lett. 56B, 473 (1975).

14. H. Kowalski and T. F. Walsh, Phys. Rev. D 14, 852 (1976). S. Okubo, Phys. Rev. D 13, 1994 (1976). S. Rudaz, Phys. Rev. D 14, 298 (1976).

15. W. Bartel et al., Phys. Lett. 64B, 483 (1976).

TABLE I

Decay modes of the $\psi(3095)$ into mesons

Topology	Decay Mode	Observed Number of Events	Efficiency	Branching Ratio
$K_S MM$	$K_S K_L$	< 4	0.23	$< 8.9 \times 10^{-5}$
$\pi^+\pi^-$	all	1.7 ± 1.7	0.040	$(1.6 \pm 1.6) \times 10^{-4}$
K^+K^-	all	1.8 ± 1.4	0.036	$(2.0 \pm 1.6) \times 10^{-4}$
$K_S K^\pm \pi^\mp$	all	126 ± 15	0.13	$(2.6 \pm 0.7) \times 10^{-3}$
	$K^o\bar{K}^{*o} + \bar{K}^o K^{*o}$	45 ± 7.8	0.044	$(2.7 \pm 0.6) \times 10^{-3}$
	$K^+K^{*-} + K^-K^{*+}$	48 ± 7.7	0.040	$(3.2 \pm 0.6) \times 10^{-3}$
	$K^o\bar{K}^{**o} + \bar{K}^o K^{**o}$	1 ± 2.7	0.007	$< 2.0 \times 10^{-3}$
	$K^+K^{**-} + K^-K^{**+}$	-1 ± 2.7	0.006	$< 1.5 \times 10^{-3}$
$\pi^+\pi^-K^+K^-$	all	205 ± 17	0.076	$(7.2 \pm 2.3) \times 10^{-3}$
	$K^{*o}\bar{K}^{**o} + \bar{K}^{*o}K^{**o}$	40 ± 8.4	0.016	$(6.7 \pm 2.6) \times 10^{-3}$
	$K^{*o}\bar{K}^{*o}$	1.5 ± 4	0.048	$< 0.5 \times 10^{-3}$
	$K^{**o}\bar{K}^{**o}$	2.5 ± 4.5	0.009	$< 2.9 \times 10^{-3}$
	$\phi\pi^+\pi^-$	23 ± 5	0.043	$(1.4 \pm 0.6) \times 10^{-3}$
	ϕf	$\lesssim 1$	0.023	$< 3.7 \times 10^{-4}$
$\pi^+\pi^-\pi^+\pi^-K^+K^-$	all	30 ± 6	0.026	$(3.1 \pm 1.3) \times 10^{-3}$
	$\phi\pi^+\pi^-\pi^+\pi^-$	$\lesssim 3$	0.013	$\lesssim 1.5 \times 10^{-3}$
$K^+K^-K^+K^-$	all	19 ± 5	0.075	$(0.7 \pm 0.3) \times 10^{-3}$
	ϕK^+K^-	14 ± 5	0.040	$(0.9 \pm 0.4) \times 10^{-3}$
	$\phi f'$	6 ± 3	0.020	$(0.8 \pm 0.5) \times 10^{-3}$
$\pi^+\pi^-K^+K^-\pi^o$	all	309 ± 50	0.073	$(1.2 \pm 0.3) \times 10^{-2}$
	ωK^+K^-	22 ± 12	0.068	$(0.8 \pm 0.5) \times 10^{-3}$
	$\omega f'$	-2 ± 2.4	0.034	$< 1.6 \times 10^{-4}$
	$\phi\eta$	5 ± 2.5	0.013	$(1.0 \pm 0.6) \times 10^{-3}$
$\pi^+\pi^-K^+K^-$ MM	$\phi\eta'$	$\lesssim 2$	0.011	$\lesssim 1.3 \times 10^{-3}$
$2(\pi^+\pi^-)\pi^o$	all†	675 ± 40†	0.17	$(4.0 \pm 1.0) \times 10^{-2}$
	$\omega\pi^+\pi^-$	348 ± 40	0.14	$(6.8 \pm 1.9) \times 10^{-3}$
	ωf	81 ± 20	0.11	$(1.9 \pm 0.8) \times 10^{-3}$
	$\rho^o A_2^o + \rho^\pm A_2^\mp$	36 ± 12	0.018	$(8.4 \pm 4.5) \times 10^{-3}$
$3(\pi^+\pi^-)\pi^o$	all†	181 ± 26†	0.062	$(2.9 \pm 0.7) \times 10^{-2}$
	$\omega 4\pi$	140 ± 30	0.044	$(8.5 \pm 3.4) \times 10^{-3}$
$4(\pi^+\pi^-)\pi^o$	all†	13 ± 4†	0.014	$(9.0 \pm 3.0) \times 10^{-3}$
$\pi^+\pi^-\pi^o$	$(\rho^o\pi^o + \rho^\pm\pi^\mp)$†	153 ± 13†	0.12	$(1.3 \pm 0.3) \times 10^{-2}$
$2(\pi^+\pi^-)$	all†	76 ± 9†	0.19	$(4.0 \pm 1.0) \times 10^{-3}$
$3(\pi^+\pi^-)$	all†	32 ± 7†	0.080	$(4.0 \pm 2.0) \times 10^{-3}$

†Taken from Ref. 3, and calculated from a smaller data sample than used in this paper. The $\pi^+\pi^-$ and K^+K^- modes were also calculated from a smaller data sample.

TABLE II

Branching ratios into general modes computed from the observation of one particular charge state of that mode

Observed mode	General mode	$\frac{BR(Observed)}{BR(General)}$ (Limits)	BR(General)(%) (Limits)	$\frac{BR(Observed)}{BR(General)}$ (Statistical Model)	BR(General)(%) (Statistical Model)
$\rho\pi$	$\rho\pi$	1	1.3 ± 0.3	1	1.3 ± 0.3
$2(\pi^+\pi^-)\pi^0$	5π	2/3	6.0 ± 1.5	2/3	6.0 ± 1.5
$3(\pi^+\pi^-)\pi^0$	7π	1/3 - 8/15	5.5 ± 1.4 to 8.7 ± 2.1	5/12	7.0 ± 1.7
$4(\pi^+\pi^-)\pi^0$	9π	0 - 16/35	$> 2.0 \pm 0.7$	7/29	3.7 ± 1.2
$\pi^\pm K^0 K^\mp$	$\pi K\bar{K}$	2/3	0.78 ± 0.21	2/3	0.78 ± 0.21
$\pi^+\pi^- K^+ K^-$	$(2\pi)K\bar{K}$	1/6 - 1/3	2.2 ± 0.7 to 4.3 ± 1.4	1/4	2.9 ± 0.9
$\pi^+\pi^-\pi^0 K^+ K^-$	$(3\pi)K\bar{K}$	1/15 - 1/2	2.4 ± 0.6 to 18.0 ± 4.5	9/40	5.3 ± 1.3
$2(\pi^+\pi^-)K^+K^-$	$(4\pi)K\bar{K}$	0 - 4/15	$> 1.2 \pm 0.5$	1/9	2.8 ± 1.2
$K^+K^-K^+K^-$	$2(K\bar{K})$	0 - 1/3	$> 0.21 \pm 0.09$	1/6	0.42 ± 0.18
Total			$> 21.6 \pm 2.4$		30.2 ± 3.3

FIGURE CAPTIONS

1. A cross-sectional view of the SLAC-LBL magnetic detector.

2. (a) Invariant mass $\pi^+\pi^-$ in two-prong events. (b) Recoiling mass against two pions with $470 < m_{\pi\pi} < 530$ MeV/c^2.

3. Mass squared of each hadron in $\psi \to h^+h^-$.

4. Dalitz plot of $\psi \to K_S K^\pm \pi^\mp$ with $K_S \to \pi^+\pi^-$.

5. Invariant masses (a) $\pi^+\pi^-K^+K^-$, (b) $K^+K^-K^+K^-$, (c) $\pi^+\pi^-\pi^+\pi^-K^+K^-$ for events with missing momentum smaller than 50 MeV/c. In (b) the shaded (unshaded) events are those with three or four (one or two) tracks identified as K by TOF.

6. Invariant mass K^+K^- in the decays (a) $\psi \to \pi^+\pi^-K^+K^-$, (b) $\psi \to K^+K^-K^+K^-$, (c) $\psi \to \pi^+\pi^-\pi^+\pi^-K^+K^-$.

7. Invariant mass $\pi^+\pi^-$ in the decays (a) $\psi \to \phi\pi^+\pi^-$, (b) $\psi \to \omega\pi^+\pi^-$. Invariant mass K^+K^- in the decays (c) $\psi \to \phi K^+K^-$, (d) $\psi \to \omega K^+K^-$. The dashed lines indicate the shape predicted by phase space corrected for detection biases.

8. Invariant mass $K^+\pi^-$ vs $K^-\pi^+$ in the decay $\psi \to \pi^+\pi^-K^+K^-$.

9. Invariant mass $K^\pm\pi^\mp$ in the decay $\psi \to \pi^+\pi^-K^+K^-$.

10. Missing mass squared recoiling against (a) $\pi^+\pi^-K^+K^-$, (b) $\pi^+\pi^-\pi^+\pi^-$, (c) $\pi^+\pi^-\pi^+\pi^-\pi^+\pi^-$.

11. (a) Invariant masses K^+K^- vs $\pi^+\pi^-\pi^0$ in the decay $\psi \to \pi^+\pi^-K^+K^-\pi^0$.
(b) Invariant masses K^+K^- vs $\pi^+\pi^-\eta$ in the decay $\psi \to \pi^+\pi^-K^+K^-\eta$.

12. Invariant mass $\pi^+\pi^-\pi^0$ in the decays (a) $\psi \to \pi^+\pi^-K^+K^-\pi^0$, (b) $\pi^+\pi^-\pi^+\pi^-\pi^0$, (c) $\pi^+\pi^-\pi^+\pi^-\pi^+\pi^-\pi^0$.

13. Invariant mass $\pi\pi$ in the decay $\psi \to \pi^+\pi^-\pi^+\pi^-\pi^0$, (a) $\pi^+\pi^-$, (b) $\pi^\pm\pi^0$, (c) $\pi^\pm\pi^0$ for those events where $700 < m_{\pi^+\pi^-} < 800$ MeV/c^2.

14. Invariant masses $\rho^0\pi$ and $\rho^\pm\pi^\mp$ in the decay $\psi \to \rho^0\rho^\pm\pi^\mp$.

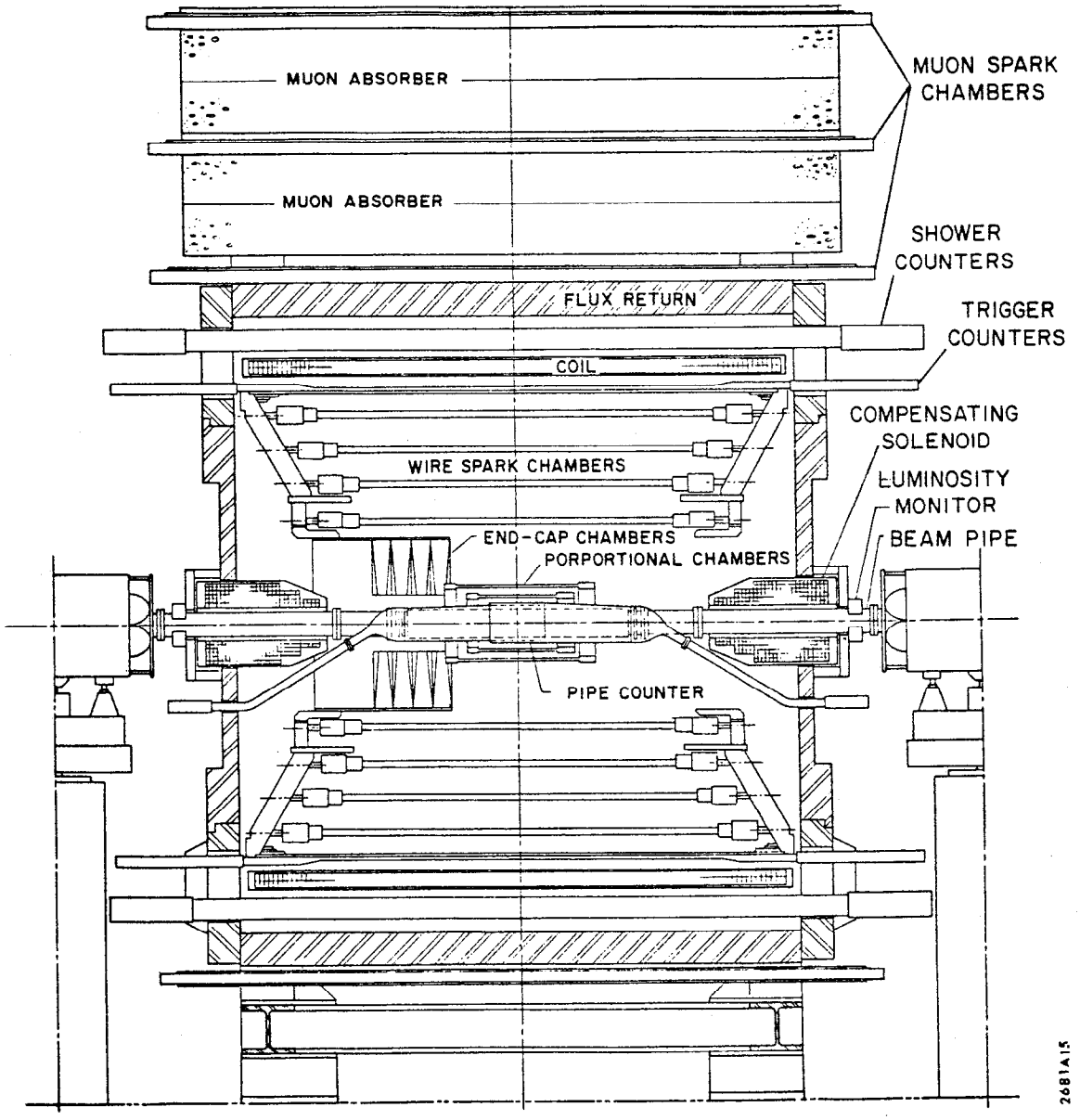
MUON ABSORBER
MUON ABSORBER
MUON SPARK CHAMBERS
SHOWER COUNTERS
FLUX RETURN
TRIGGER COUNTERS
COIL
COMPENSATING SOLENOID
WIRE SPARK CHAMBERS
LUMINOSITY MONITOR
END-CAP CHAMBERS
PORPORTIONAL CHAMBERS
BEAM PIPE
PIPE COUNTER
2681A15

Fig. 1

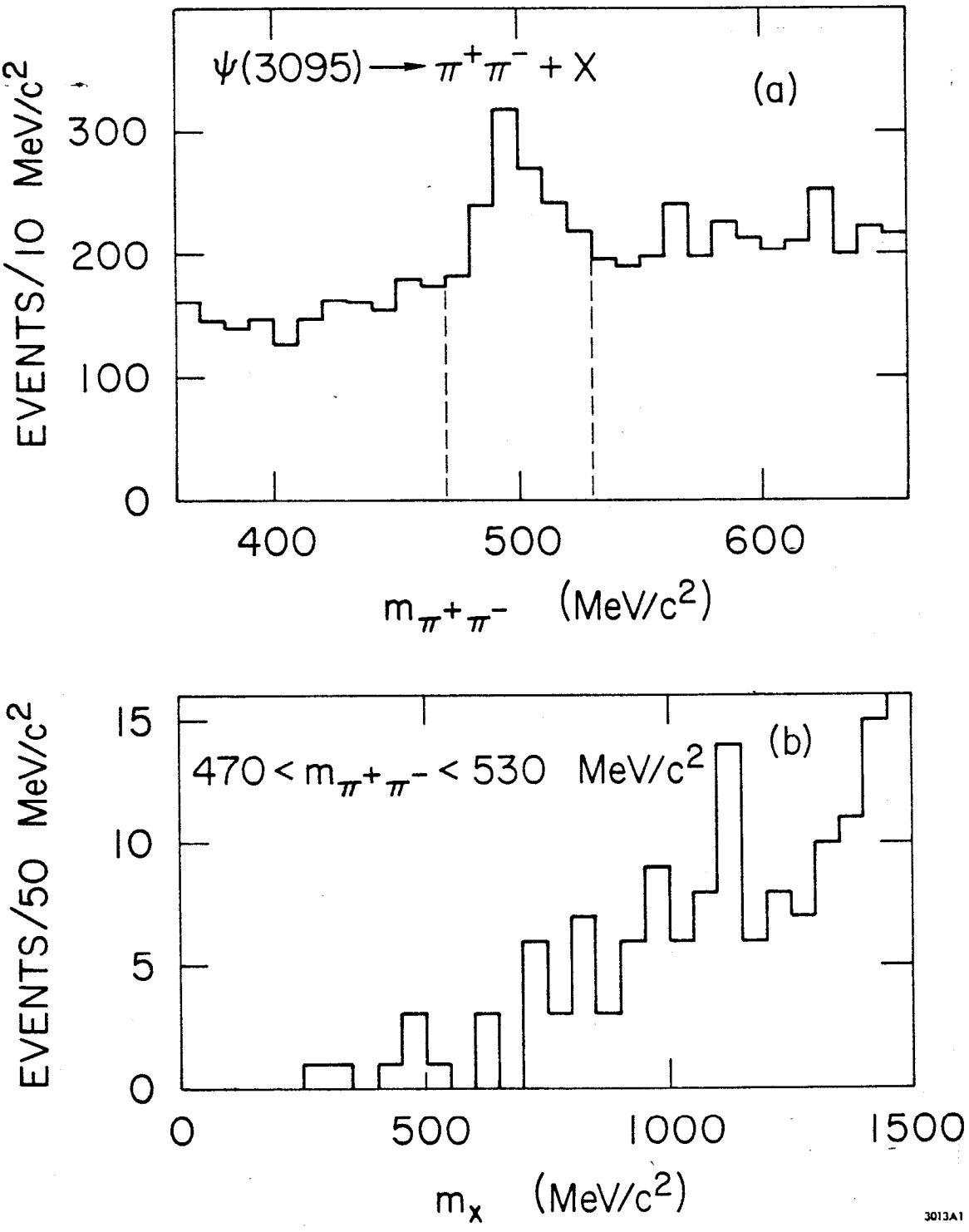
ψ(3095) → π+π− + X
(a)
EVENTS/10 MeV/c2
300
200
100
0
400
500
600
mπ+π− (MeV/c2)
EVENTS/50 MeV/c2
15
10
5
0
(b)
470 < mπ+π− < 530 MeV/c2
0
500
1000
1500
mx (MeV/c2)
3013A1

Fig. 2

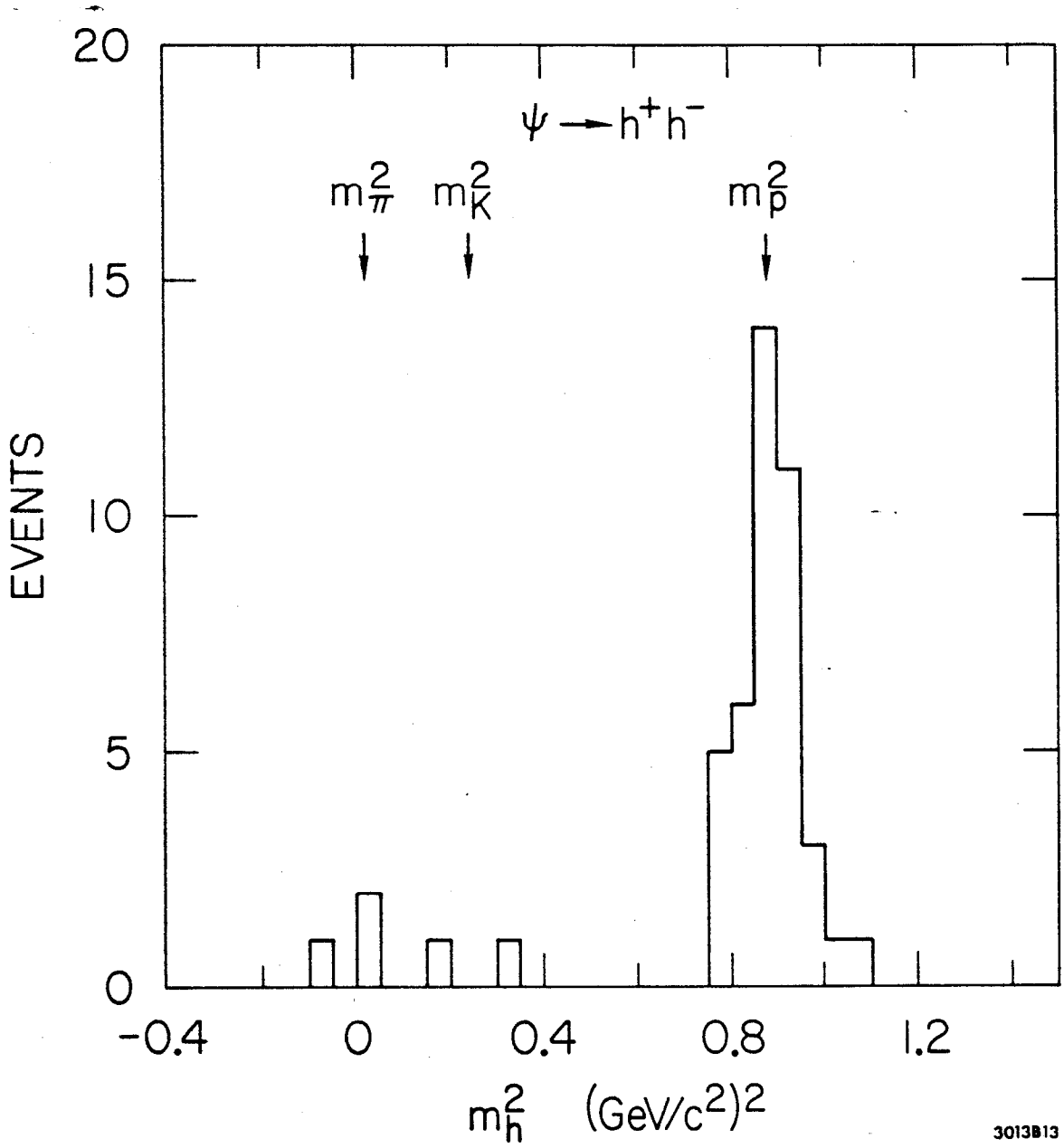
20
15
10
5
0
EVENTS
$\psi \rightarrow h^+h^-$
m_π^2
m_K^2
m_p^2
-0.4
0
0.4
0.8
1.2
m_h^2 $(GeV/c^2)^2$
3013B13

Fig. 3

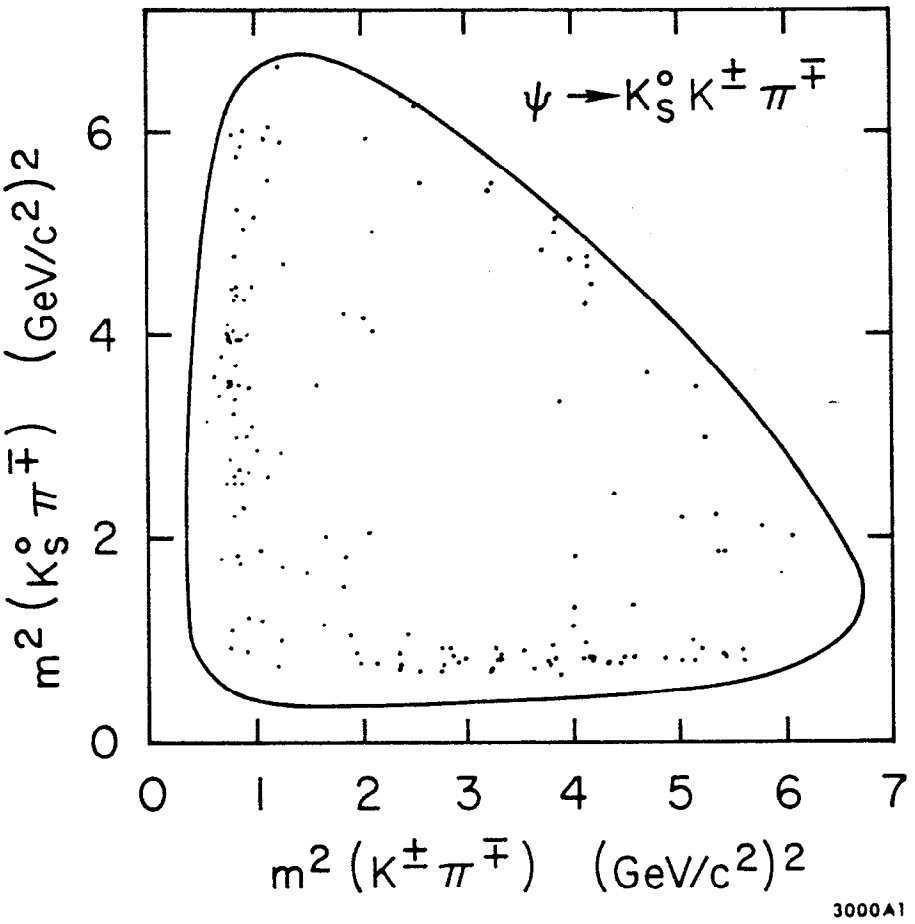
$\psi \rightarrow K_S^0 K^{\pm} \pi^{\mp}$
$m^2 (K_S^0 \pi^{\mp})$ $(GeV/c^2)^2$
$m^2 (K^{\pm} \pi^{\mp})$ $(GeV/c^2)^2$
0
1
2
3
4
5
6
7
3000A1

Fig. 4

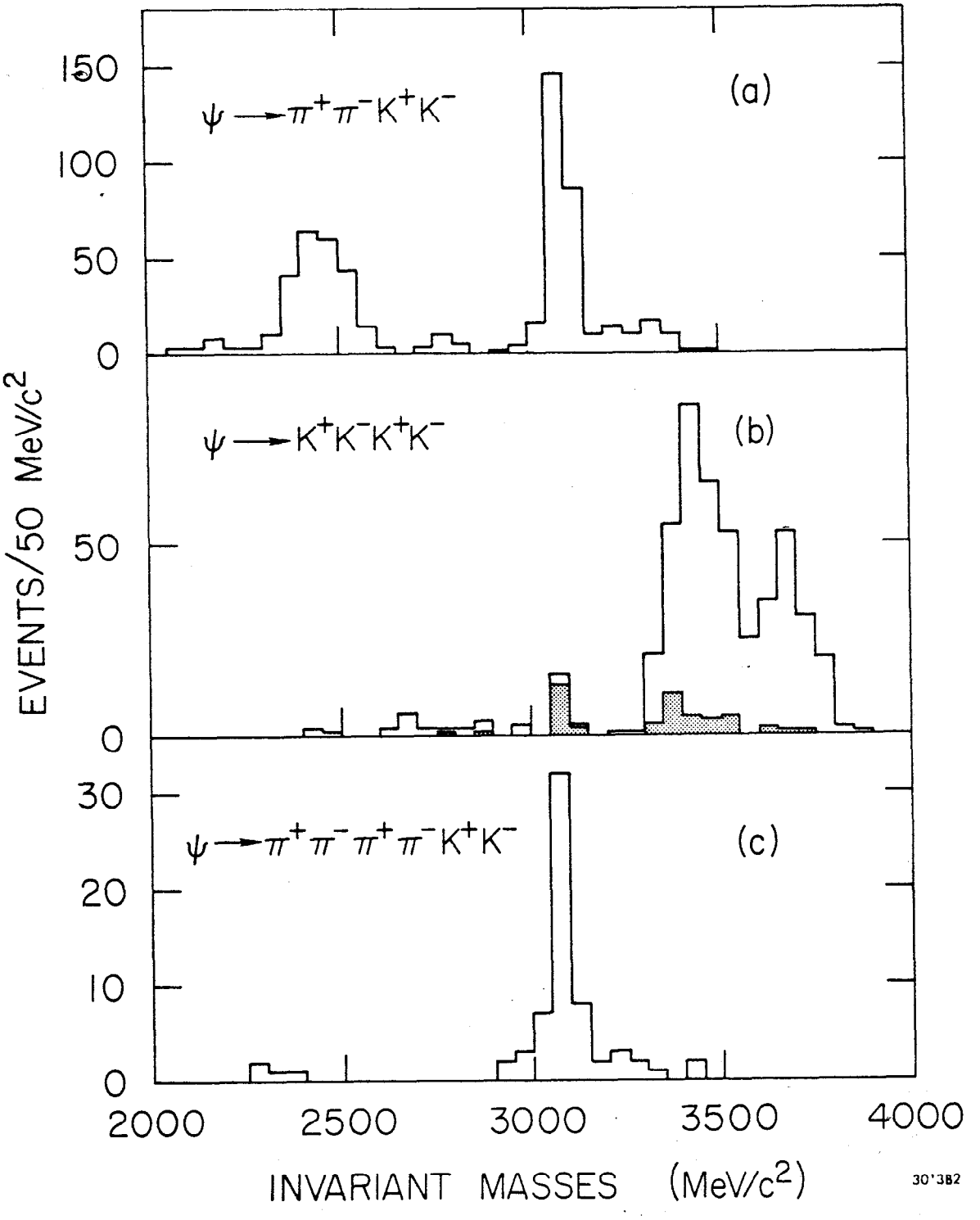
150
100
50
0
ψ → π⁺π⁻K⁺K⁻
(a)
50
0
ψ → K⁺K⁻K⁺K⁻
(b)
30
20
10
0
ψ → π⁺π⁻π⁺π⁻K⁺K⁻
(c)
EVENTS/50 MeV/c²
2000
2500
3000
3500
4000
INVARIANT MASSES (MeV/c²)
30'382

Fig. 5

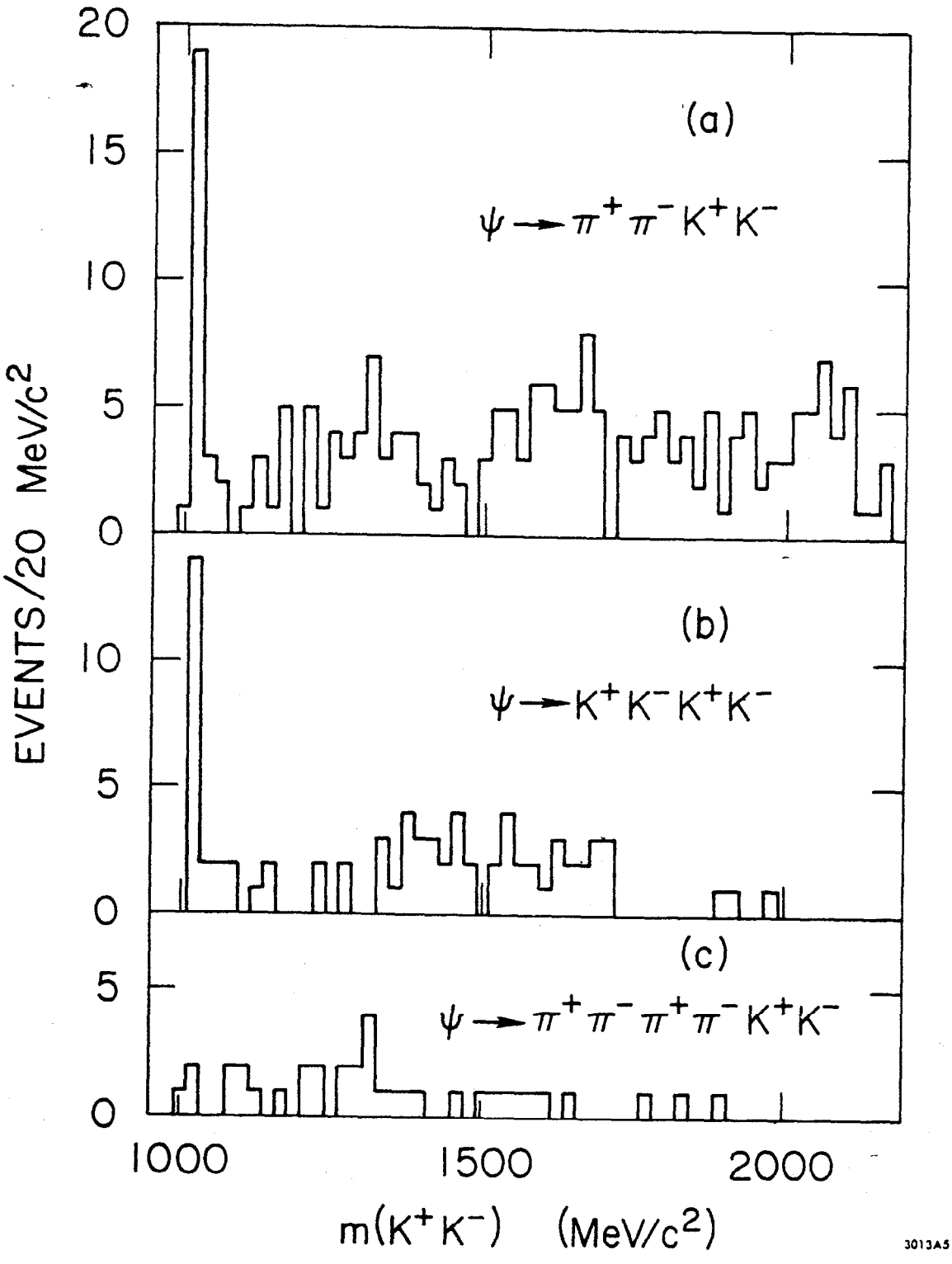
20
15
10
5
0
(a)
$\psi \rightarrow \pi^+\pi^-K^+K^-$
10
5
0
(b)
$\psi \rightarrow K^+K^-K^+K^-$
5
0
(c)
$\psi \rightarrow \pi^+\pi^-\pi^+\pi^-K^+K^-$
EVENTS/20 MeV/c^2
1000
1500
2000
m(K$^+$K$^-$) (MeV/c^2)
3013A5

Fig. 6

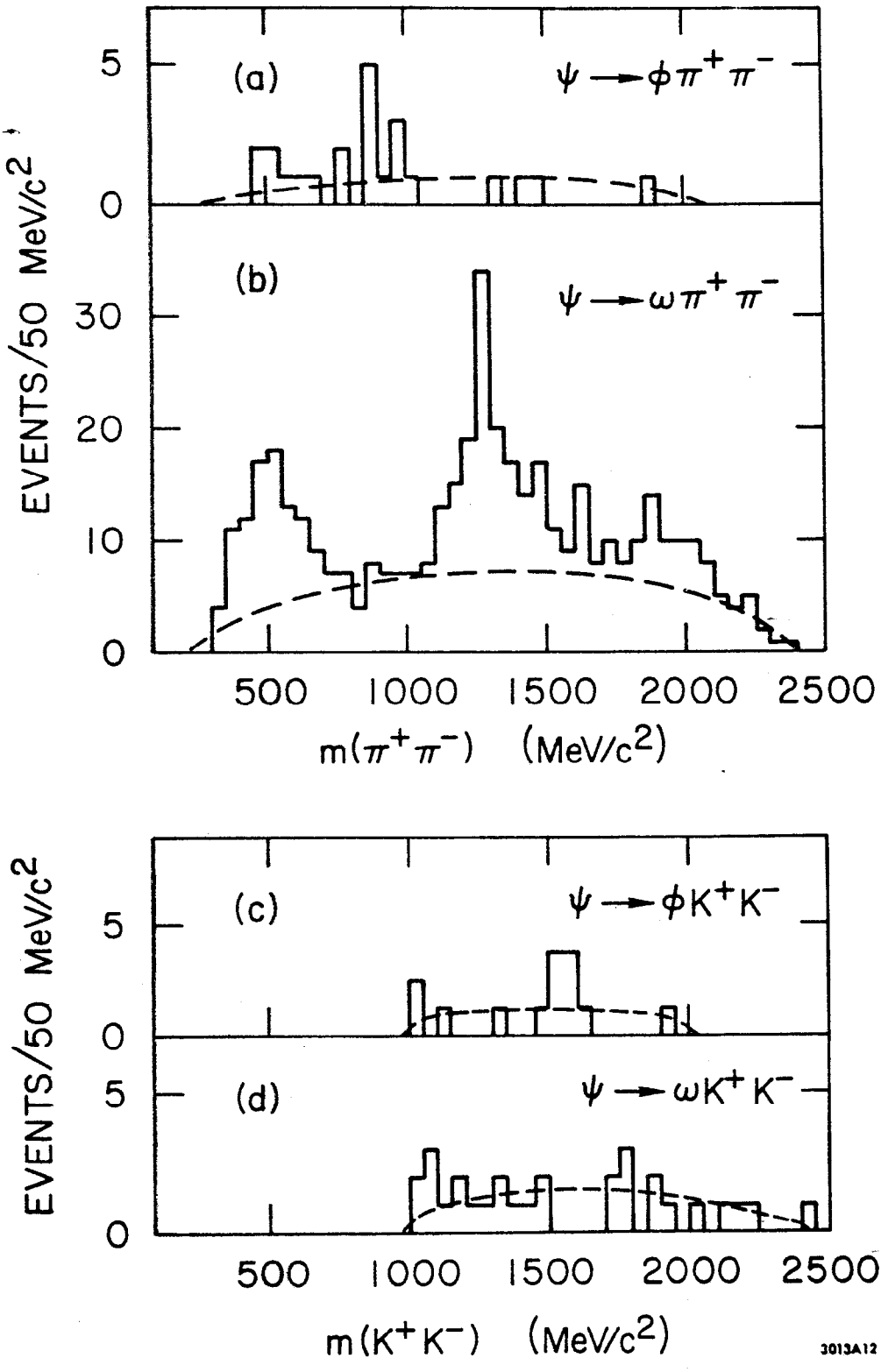
(a)
$\psi \rightarrow \phi\pi^+\pi^-$
(b)
$\psi \rightarrow \omega\pi^+\pi^-$
EVENTS/50 MeV/c^2
5
0
30
20
10
0
500
1000
1500
2000
2500
m($\pi^+\pi^-$) (MeV/c^2)
(c)
$\psi \rightarrow \phi K^+K^-$
(d)
$\psi \rightarrow \omega K^+K^-$
EVENTS/50 MeV/c^2
5
0
5
0
500
1000
1500
2000
2500
m(K^+K^-) (MeV/c^2)
3013A12

Fig. 7

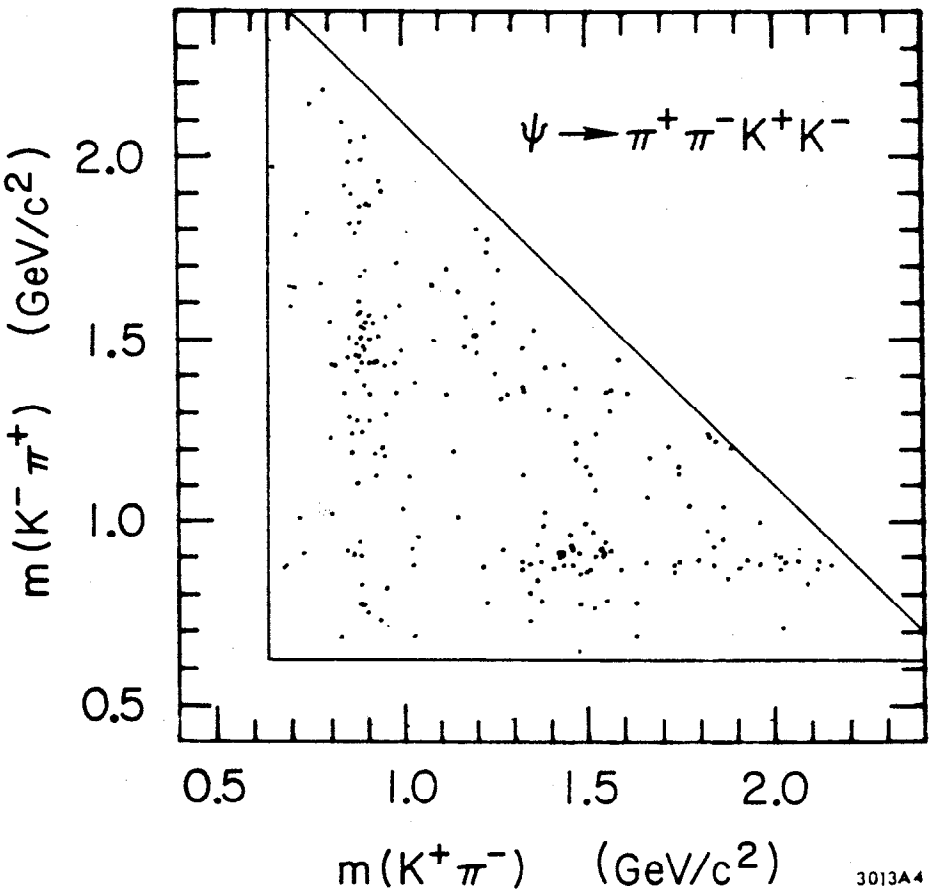
$\psi \rightarrow \pi^+\pi^-K^+K^-$
2.0
1.5
1.0
0.5
$m(K^-\pi^+)$ (GeV/c^2)
0.5
1.0
1.5
2.0
$m(K^+\pi^-)$ (GeV/c^2)
3013A4

Fig. 8

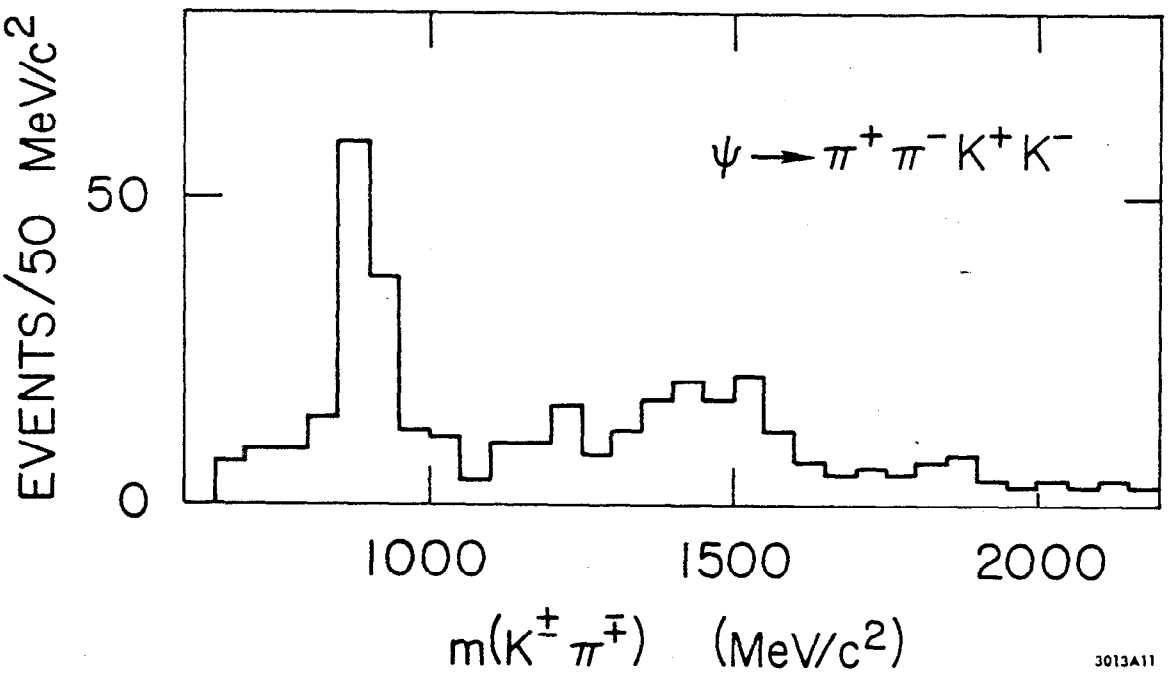

Fig. 9

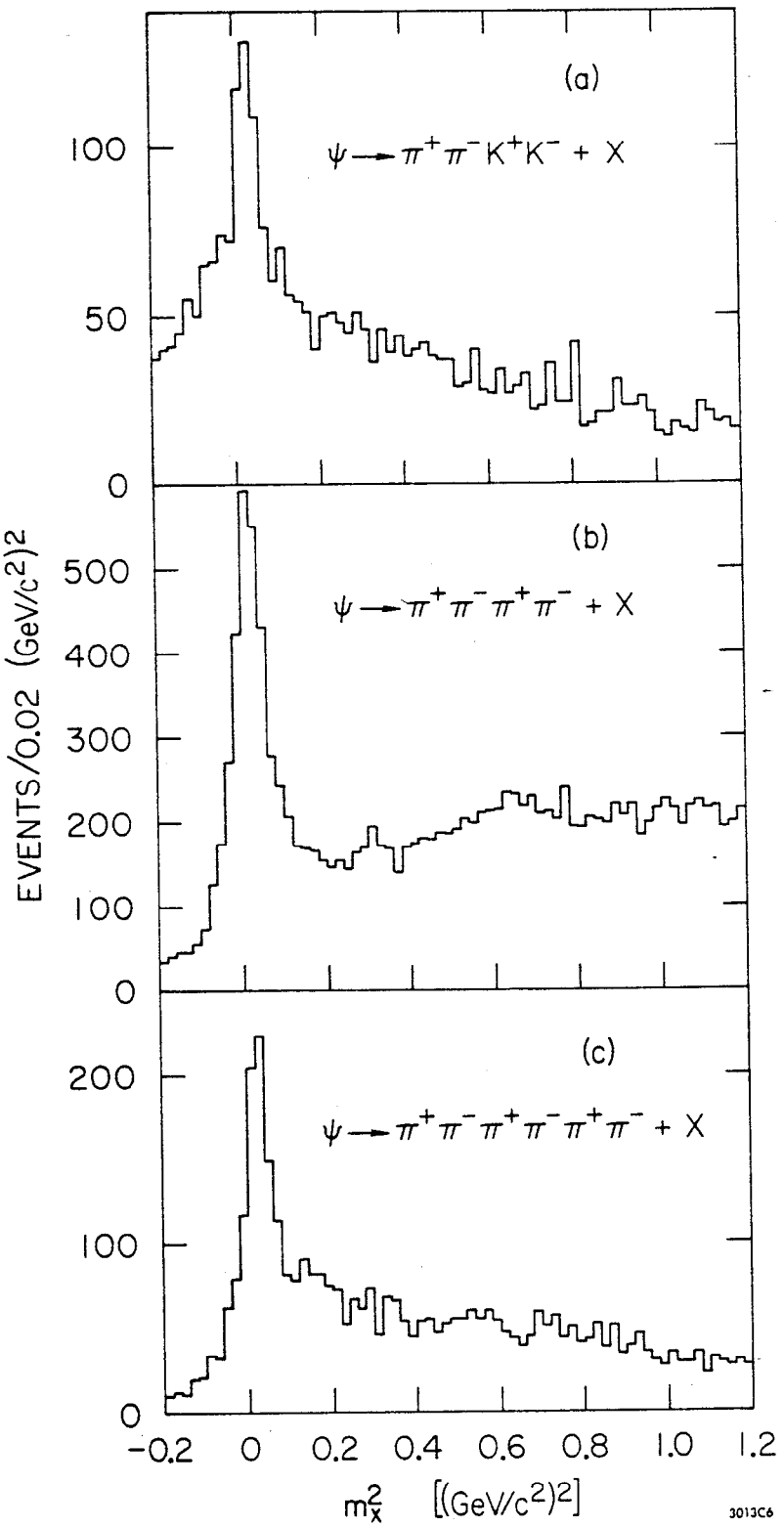
(a)
$\psi \rightarrow \pi^+\pi^-K^+K^- + X$
(b)
$\psi \rightarrow \pi^+\pi^-\pi^+\pi^- + X$
(c)
$\psi \rightarrow \pi^+\pi^-\pi^+\pi^-\pi^+\pi^- + X$
EVENTS/0.02 (GeV/c²)²
100
50
0
500
400
300
200
100
0
200
100
0
-0.2
0
0.2
0.4
0.6
0.8
1.0
1.2
m_x^2 [(GeV/c²)²]
3013C6

Fig. 10

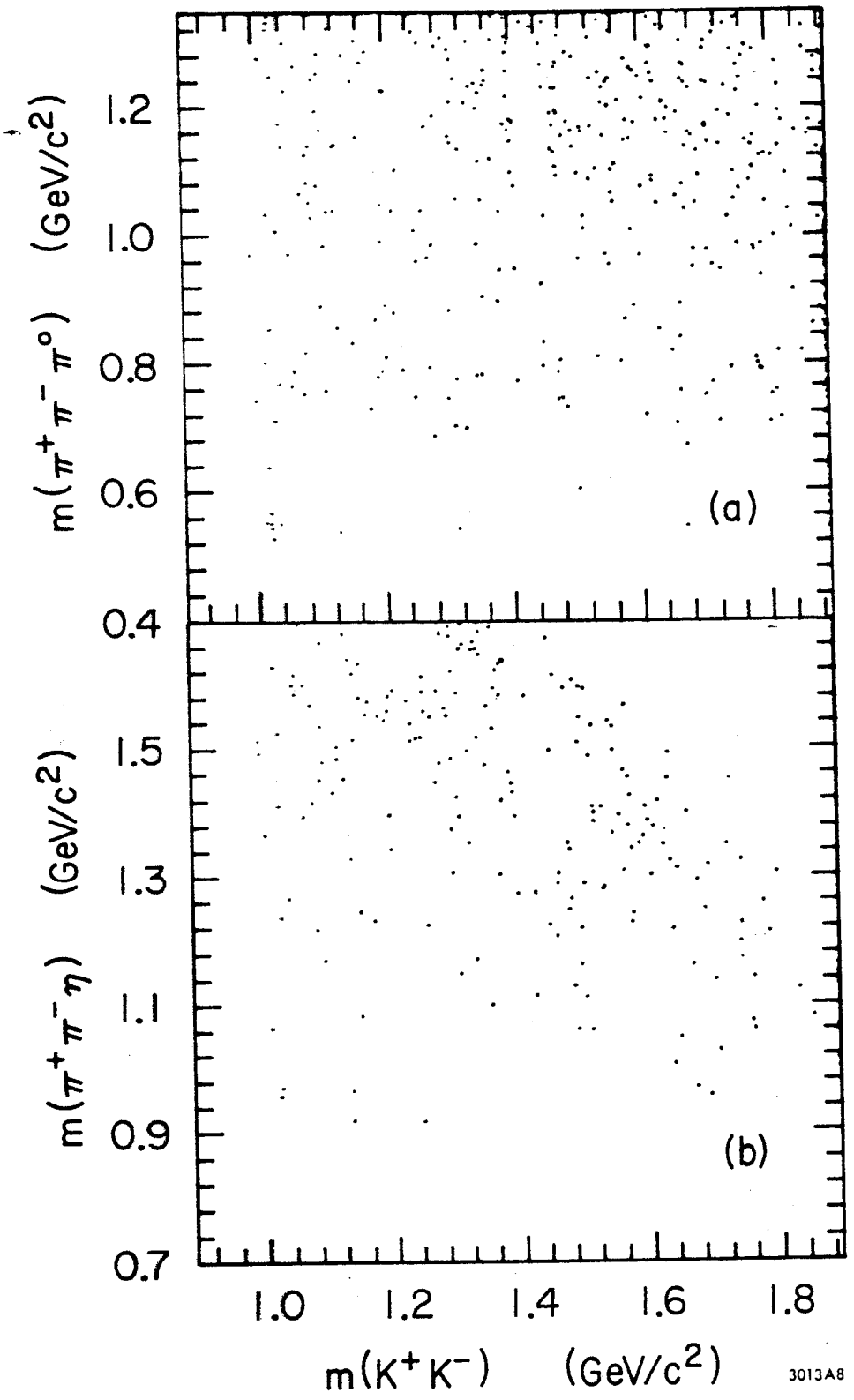
1.2
1.0
0.8
0.6
0.4
m(π+π−π°) (GeV/c2)
(a)
1.5
1.3
1.1
0.9
0.7
m(π+π−η) (GeV/c2)
(b)
1.0
1.2
1.4
1.6
1.8
m(K+K−) (GeV/c2)
3013A8

Fig. 11

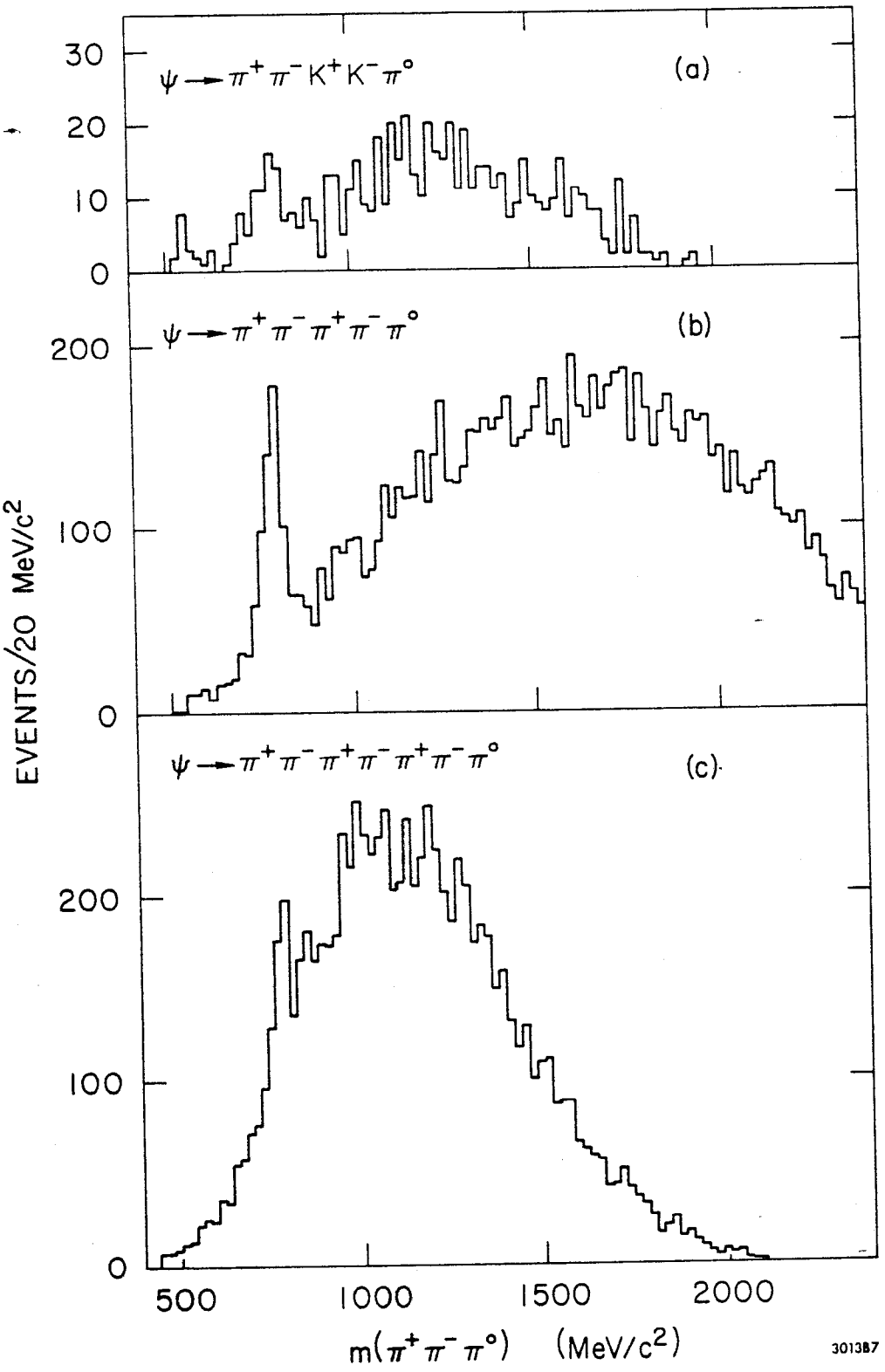
ψ → π⁺π⁻K⁺K⁻π°
(a)
ψ → π⁺π⁻π⁺π⁻π°
(b)
ψ → π⁺π⁻π⁺π⁻π⁺π⁻π°
(c)
EVENTS/20 MeV/c²
m(π⁺π⁻π°) (MeV/c²)
30
20
10
0
200
100
0
200
100
0
500
1000
1500
2000
301387

Fig. 12

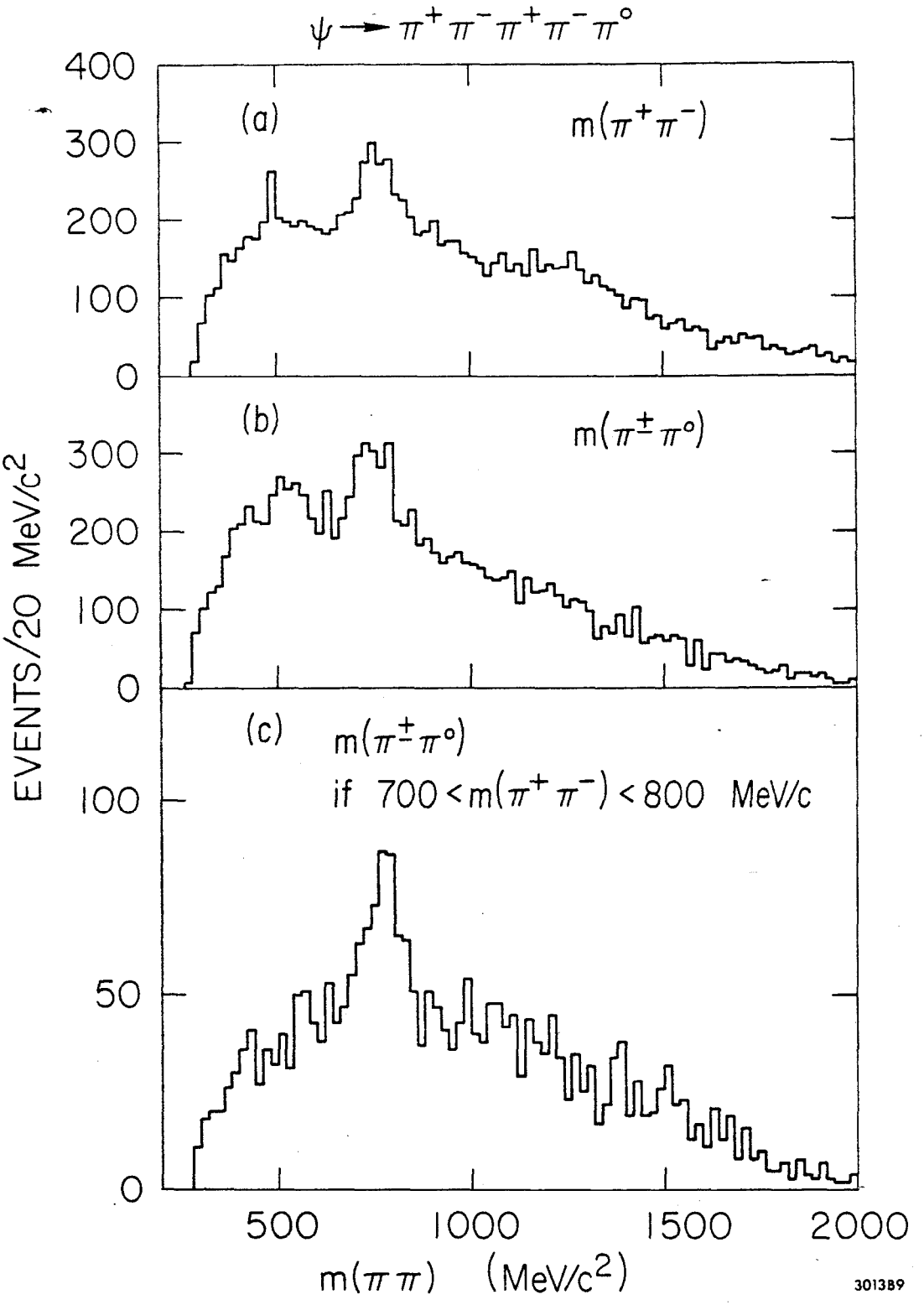
$\psi \rightarrow \pi^+\pi^-\pi^+\pi^-\pi^\circ$
(a)
$m(\pi^+\pi^-)$
(b)
$m(\pi^\pm\pi^\circ)$
(c)
$m(\pi^\pm\pi^\circ)$
if $700 < m(\pi^+\pi^-) < 800$ MeV/c
EVENTS/20 MeV/c^2
400
300
200
100
0
300
200
100
0
100
50
0
500
1000
1500
2000
$m(\pi\pi)$ (MeV/c^2)
301389

Fig. 13

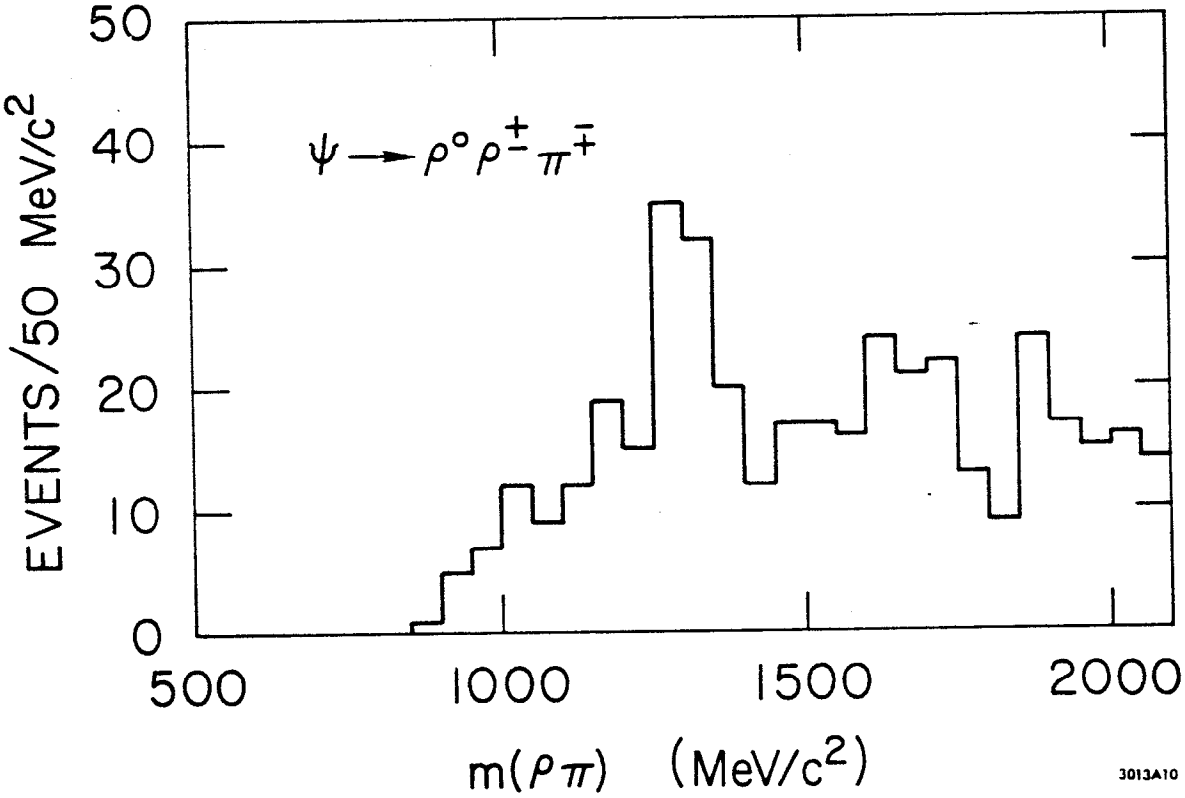
50
40
30
20
10
0
EVENTS/50 MeV/c²
ψ → ρ° ρ± π∓
500
1000
1500
2000
m(ρπ) (MeV/c²)
3013A10

Fig. 14